North American climate of the last millennium: Underground temperatures and model comparison

M. Bruce Stevens,[1] J. Fidel González-Rouco,[2] and Hugo Beltrami[1]

Received 5 October 2006; revised 18 August 2007; accepted 9 October 2007; published 5 February 2008.

[1] General circulation models (GCMs) are currently able to provide physically consistent simulations of millennial climate variability in which estimations of external forcing factors are incorporated as boundary conditions. Climate reconstruction attempts to recover as faithfully as possible past climate variability using a variety of independent and climate-sensitive sources of information. By deriving strategies of comparison between GCM simulations and proxy data, or directly recorded data such as subsurface thermal profiles, the agreement between model and observations can be assessed. Thermal profiles obtained from the boreholes of North America were grouped into eight geographically discrete ensembles and averaged to form robust, representative profiles. The gridded output from the three distinct integrations of the GCM ECHO-g were similarly averaged by region. These simulated, millennial, paleoclimatic histories were then forward modeled to arrive at the subsurface thermal profiles that would result from the temperature trends at the surface. These forward modeled profiles were then compared with the borehole average thermal anomaly profile in each region. In most of the regions studied, the externally forced runs from ECHO-g are in better agreement with underground temperature anomalies than with the control run, suggesting that boreholes are sensitive to external forcing. Not only do ECHO-g simulations demonstrate better agreement with borehole data when considering variable external forcing factors, but ECHO-g also appears to broadly describe qualitative aspects of long-term climatic trends at a regional scale.

Citation: Stevens, M. B., J. F. González-Rouco, and H. Beltrami (2008), North American climate of the last millennium: Underground temperatures and model comparison, *J. Geophys. Res.*, *113*, F01008, doi:10.1029/2006JF000705.

1. Introduction

[2] Recent work indicates that all of the Earth's climate subsystems have gained heat in the last 50 years [*Levitus et al.*, 2001, 2005; *Beltrami*, 2002a; *Beltrami et al.*, 2002, 2006a], suggesting that the present warming has a global character. In addition, evidence shows that this warming is in fact influenced by anthropogenic activities [*Intergovernmental Panel on Climate Change*, 2001] and seems unprecedented since 1400 CE [*Intergovernmental Panel on Climate Change*, 2007a, 2007b; *Hansen et al.*, 2006; *North et al.*, 2006].

[3] Assessment of the relevance of observed warming in a wider temporal context and its possible link to human activities has encouraged studies of climate variability and change through the last millennium. Research has been focused both on model simulations of the past climate evolution and on statistical reconstruction using proxy sources such as *Jones and Mann* [2004]. The modeling approach has made use of models with different degrees of complexity to simulate the response of the climate system to variations in external forcings, e.g., solar variability, volcanic activity, variable greenhouse gas concentrations, vegetation changes, etc. This approach includes Energy Balance Models (EBM) [*Crowley*, 2000; *Hegerl et al.*, 2006]; Earth-System Models of Intermediate Complexity (EMIC) [*Bauer et al.*, 2003; *Montoya et al.*, 2005; *Bauer and Claussen*, 2006]; and state-of-the-art General Circulation Models (GCM) [*Cubasch et al.*, 1997; *Zorita et al.*, 2004]. In turn, reconstructions of the climate history through the last millennium have used various proxy indicators and methodologies. These studies have focused on a wide array of spatial scales, from local and regional [*Cook*, 1995] to hemispherical and global [*Esper et al.*, 2002; *Jones and Mann*, 2004; *Moberg et al.*, 2005]. In an ideal situation, model simulations and climate reconstructions should converge on their assessments of past climate variability. Though considerable progress has been made in the last decade, this agreement is still hampered by many uncertainties that affect both climate reconstructions and model simulations.

[4] For the purposes of reconstructing climate on a centennial to millennial timescale, borehole temperature data appear a good source of information [*Pollack and Huang*, 2000]. Unlike proxy indicators, temperature data retrieved from boreholes record a direct signal of long-term trends of past climate, because underground temperatures

[1] Environmental Sciences Research Centre, St. Francis Xavier University, Antigonish, Nova Scotia, Canada.
[2] Departamento de Astrofísica y CC. de la Atmósfera, Universidad Complutense de Madrid, Madrid, Spain.

0148-0227/08/2006JF000705

are directly related to the SAT history [*Harris and Chapman*, 2001; *Pollack and Smerdon*, 2004; *Beltrami et al.*, 2005; *González-Rouco et al.*, 2003, 2006]. The thermal signal penetrating the surface propagates underground predominantly via conduction through the strongly coupled air-ground interface, and its amplitude is attenuated and phase shifted with depth and time [*Beltrami and Kellman*, 2003; *Pollack et al.*, 2005; *Smerdon and Stieglitz*, 2006; *Smerdon et al.*, 2006]. In the absence of long-term changes in ground surface temperature, the subsurface profile shows a uniform, or "quasi-steady state" temperature at depths below the regime of seasonal oscillations. For typical subsurface thermal parameters, the signal due to annual variation is insignificant deeper than about 20 m.

[5] Low-frequency surface temperature changes propagate into the subsurface, and are superimposed as perturbations to the quasi-steady state subsurface temperature profile. The extent to which these perturbations are present in the subsurface is proportional to the duration and magnitude of the climatic event at the surface. This feature gives boreholes the unique property of accurately preserving the long-term trends in climatic signal, while removing high-frequency variability inherent to most meteorological records [*Pollack and Huang*, 2000; *Clauser and Mareschal*, 1995; *Beltrami et al.*, 2002; *Harris and Chapman*, 2001, 2005; *Pollack and Smerdon*, 2004; *Smerdon and Stieglitz*, 2006].

[6] There has been a great deal of controversy regarding the suitability of boreholes as indicators of past climate. The now well-known Mann-Bradley-Hughes (MBH) reconstruction [*Mann et al.*, 1999] used multiproxy data to simulate the Northern Hemispheric average temperature for the past 1000 years. The MBH reconstruction emphasizes a gradual decline in temperature from the year 1000 to about 1700, followed by a rapid increase from 1700 to present. This multiproxy reconstruction shows a significant deviation from Northern hemispheric borehole reconstructions [*Huang et al.*, 2000; *Harris and Chapman*, 2001; *Beltrami and Bourlon*, 2004]. However, more recent studies have yielded results that solidify the credibility of boreholes as indicators of past climate [*Esper et al.*, 2002, 2004; *Pollack and Smerdon*, 2004; *Moberg et al.*, 2005; *González-Rouco et al.*, 2003, 2006; *Harris and Chapman*, 2005; *Hegerl et al.*, 2007].

[7] In this paper, simulations of the last millennium using the ECHO-g climate model [*González-Rouco et al.*, 2003, 2006] are compared to observed subsurface temperature data from boreholes. Using the model temperature output as an upper boundary condition at the ground surface, the forward heat conduction problem is solved to simulate the underground thermal regime at each model grid point. The analysis is carried out by simulating the transient underground thermal regime at the regional scale in the model simulations and comparing it to the measured subsurface perturbations from geothermal data. The North American borehole database was chosen because of the high density and average depth of borehole logs.

[8] It is well known that individual borehole temperature log analysis is not the preferred method for inferring climate change because of the possibility of microclimatic effects due to a variety of transient nonclimatic surface conditions such as deforestation [*Nitoiu and Beltrami*, 2005; *Ferguson and Beltrami*, 2006], irrigation cooling effects (ICEs) [*Kueppers et al.*, 2007], groundwater flow [*Harris and Chapman*, 1995; *Bodri and Cermak*, 2005; *Ferguson et al.*, 2006], topographic effects [*Kohl*, 1998, 1999], and freezing phenomena [*Zhang*, 2005; *Mottaghy and Rath*, 2006]. In order to arrive at robust estimates of past climatic changes, climate inferences from subsurface temperatures are carried out for ensembles of temperature logs representing a large region [*Beltrami and Mareschal*, 1992; *Beltrami et al.*, 1992, 1997; *Clauser and Mareschal*, 1995; *Pollack et al.*, 1996]. Random noise present in the individual logs will tend to cancel, reinforcing the climatic signal. Accordingly, gridded temperature output from ECHO-g was also spatially averaged over these same regions for the purpose of comparison.

[9] Observed subsurface temperature anomalies can be compared to model paleoclimatic simulations. However, the comparison requires the selection of a reference period against which anomalies are referenced [*Beltrami et al.*, 2006b]. In our case, such selection is not evident both because boreholes integrate the influence of climatic events before the start of the 1000-year ECHO-g GCM paleoclimatic simulation used here, and also because these simulations of the last millennium do not necessarily yield an exact representation of past temperatures.

[10] We compare observed and simulated subsurface temperature anomalies, avoiding the selection of a single reference period. This can be done because choosing a reference period is the same as setting a reference level of average past temperatures with respect to which the anomalies can be calculated. Instead, scanning over a range of all possible mean temperature reference levels yields a set of anomaly profiles to compare with observed thermal perturbation profiles. This is used to explore whether the observed subsurface temperature anomalies in each of the regions considered here can be explained solely by the climate system internal dynamics as in the control simulation, or whether the subsurface anomalies are better explained by the simulations that include external, natural and anthropogenic forcings. We assess subsurface anomalies using a set of criteria to strengthen our model and observation comparison.

[11] Although we do not claim attribution of climatic change to any particular anthropogenic or natural forcing, our results indicate that ECHO-g is in better agreement with past climate at the regional level as inferred from borehole temperatures when taking into account natural and anthropogenic external forcings than in their absence. This implies that borehole temperatures are sensitive to external forcings such as changing greenhouse gas concentrations and solar radiation, and that the combined effects of these forcings are recorded in the subsurface thermal profile.

1.1. General Circulation Model ECHO-g: Model Description

[12] Model data were obtained from climate simulations produced with the ECHO-g atmosphere-ocean general circulation model (GCM). ECHO-g [*Legutke and Voss*, 1999] consists of the atmospheric and ocean GCM components ECHAM4 and HOPE-g. ECHAM4 [*Roeckner et al.*, 1996] is used with a T30 horizontal resolution (approximately 3.75°) and 19 vertical levels. HOPE-g [*Wolff et al.*, 1997] is used with a T42 (approximately 2.8°) horizontal resolution which varies toward the equator where it reaches a mini-

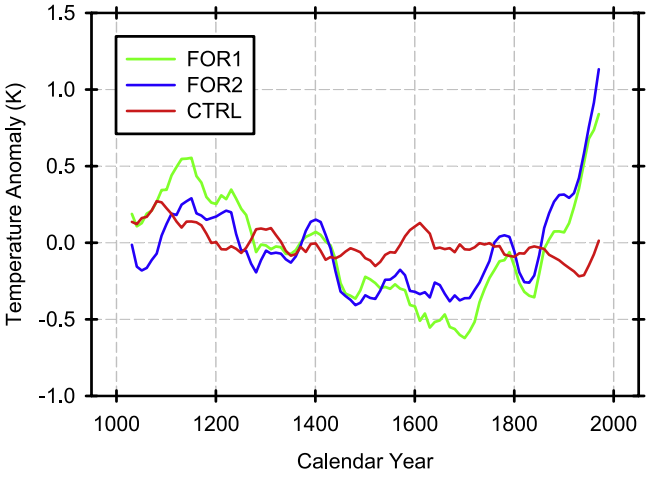

Figure 1. Summary of Northern Hemispheric average temperature histories for the three integrations of ECHO-g.

mum grid point separation of 0.5° for an improved representation of equatorial and tropical ocean currents. Vertical discretization for the ocean incorporates 20 levels.

[13] In order to avoid climate drift, heat and freshwater flux adjustments were applied to the ocean. These fluxes were diagnosed in a coupled spin-up integration with restoring terms that drive the sea surface temperature and sea surface salinity to their climatological observed values. These flux adjustments are constant in time through the integration and their global contribution is zero.

[14] The surface scheme comprises a soil model, hydrology, snow cover physics and vegetation effects on surface evapotranspiration among others. The soil model, an extension of *Warrilow et al.* [1986], is a five layer finite difference approximation of the diffusion equation which operates on the T30 land-sea mask grid of ECHAM4. Ground temperatures are simulated at five levels with depths at 0.06 m, 0.32 m, 1.23 m, 4.13 m, and 9.83 m. At 9.83 m, ECHO-g has a bottom boundary that currently ranks among the deepest for state-of-the-art GCMs. This is very important, as a bottom boundary that is too shallow could allow heat propagating downward in the subsurface to "reflect" off the boundary, resulting in nonphysical heat transport and storage in the subsurface [*Smerdon and Stieglitz*, 2006; *Stevens et al.*, 2007]. A zero heat flux is prescribed at the bottom boundary in order to ensure that no artificial heat sources and sinks may affect the energy balance.

[15] This work makes use of three integrations with the ECHO-g GCM: A 1000-year control simulation (CTRL) in which external forcing was fixed to the values of present climate, and two forced simulations (FOR1,2) covering the period 1000 to 1990 CE These forced simulations were produced by driving the model with estimations of external forcing factors: greenhouse gas concentrations in the atmosphere, solar irradiance and an estimation of the radiative effects of stratospheric volcanic aerosols. The atmospheric concentrations of CO_2 and CH_4 were estimated from analysis of air bubbles in Antarctica ice cores [*Etheridge et al.*, 1996, 1998]. Concentrations of N_2O were used as in previous scenario experiments with this model [*Roeckner et al.*, 1999]: fixed 276.7 ppb before 1860 CE and the historical evolution from 1860 to 1990 CE which was adjusted from *Battle et al.* [1996]. The past variations of solar irradiance were derived from observations of sunspots and concentrations of the ^{10}BE cosmogenic isotope [*Lean et al.*, 1995; *Crowley*, 2000]. Estimations for the last 1000 years provided by *Crowley* [2000] were translated to variations in the solar constant. The effect of volcanic aerosols is incorporated as global effective variations of the annual values of the solar constant obtained from short wave radiative forcing changes [*Crowley*, 2000]. Information on the location and timing of eruptions within the year is not taken into account. No changes in atmospheric aerosol concentration were considered, nor changes in vegetation cover or land use.

[16] Further description and illustration of external forcing as well as results from these simulations can be found in *von Storch et al.* [2004], *Zorita et al.* [2003, 2004, 2005], *González-Rouco et al.* [2003, 2006], and *Beltrami et al.* [2006b]. Figure 1 shows a summary of the Northern Hemispheric average temperature history for the three integrations of ECHO-g.

[17] With regard to the development of the GCM integrations, CTRL was made in a CRAY C90 machine of the Hamburg DKRZ (German Climate Computing Center). FOR1 and FOR2 were carried out in a posterior NEC machine of the DKRZ. FOR1 was started from initial conditions extracted after a 100-year continuation of the CTRL in the NEC system. After this 100-year period, the simulation was driven for 50 years to the conditions of 1000 CE and allowed 50 years more with these constant external forcing values. After this 100-year spin down period, the external forcing values were changed year by year according to the estimations of forcing through the last millennium specified above. Conversely, FOR2 was initiated from relatively cold conditions using restart files from the year 1700 CE in FOR1 and allowing it a 50-year interval to adjust to the conditions of year 1000 CE, plus 50 additional years with fixed 1000 CE values of external forcing. The length of these spin down periods was decided as a compromise between computing time costs and allowing the system some time to adapt to the new external forcing values. *Goosse et al.* [2005] and *Osborn et al.* [2006] suggest that FOR1 is unusually warm in comparison with other model simulations, a feature that can be related to rather warm initial conditions and the relatively short spin down. Although the possibility of some initial imbalance can also not be ruled out in FOR2, the level of medieval warming simulated in FOR2 can be supported with results from other more recent state-of-the-art GCM [*Mann et al.*, 2005] and EMIC simulations [*Goosse et al.*, 2005] which deliver a very similar climate evolution through the last millennium.

[18] The interpretation of these simulations should also be bounded by the external forcing factors which are taken into consideration. Sulphate aerosols or vegetation changes are not incorporated into the development of these simulations, and some relative cooling effect from these forcing factors [*Bauer et al.*, 2003; *Osborn et al.*, 2006] should be expected that would damp the warming trends throughout the 20th century. Thus results should be viewed within the frame of unknowns sketched above.

[19] This work compares the temperature response simulated using a specific model and set of forcings and observational evidence from borehole temperature profiles.

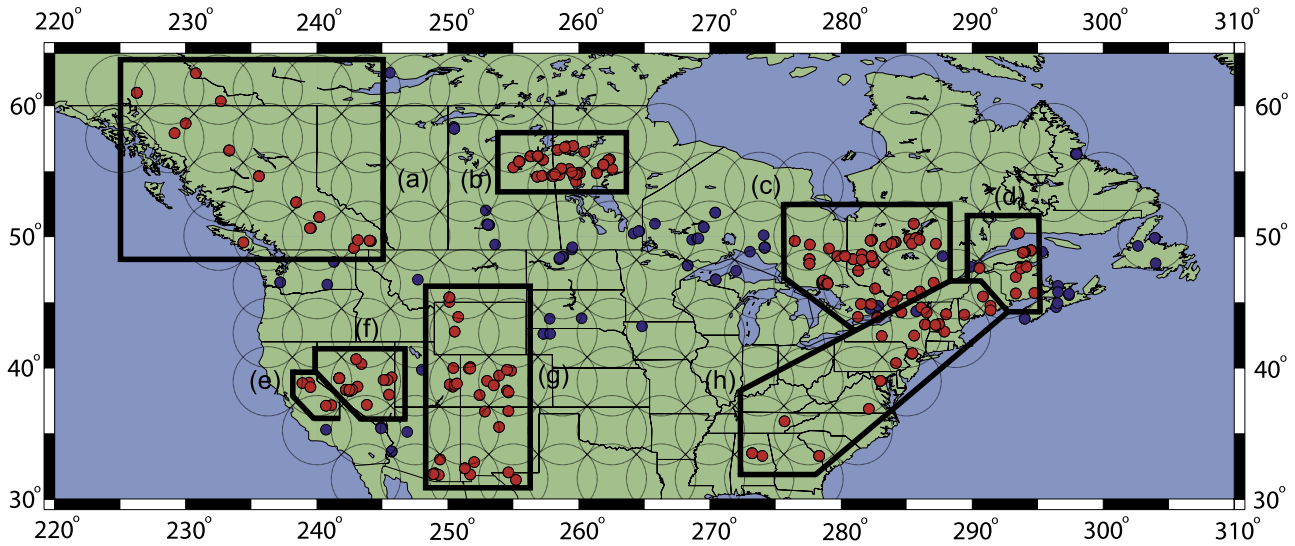

Figure 2. Spatial distribution of North America's boreholes, including those used in the study (red dots) and those omitted (blue dots); model output grid points are located at the center of hollow circles. The eight geographical regions of interest are bounded: (a) Pacific Canada, (b) western Canada, (c) central Canada, (d) Atlantic Canada, (e) California, (f) Nevada, (g) intermountain West, and (h) eastern United States.

Since the available model runs incorporate forcings from both natural and anthropogenic sources, there can be no conclusions drawn about the effects of individual forcing factors on subsurface temperature perturbations. However, it is possible to determine whether changing values of forcing factors are required to account for North American climate variability through the last millennium as recorded in borehole temperature profiles.

1.2. Data Sets

[20] The set of data used as the basis for this work includes 287 temperature versus depth profiles obtained from boreholes in North America. These boreholes range in maximum depth from 200 to 700 meters, and are located between 30° and 65°N latitude, and 60° and 140°W longitude. These boreholes are divided into eight geographical regions to capitalize on areas of high data density, and to limit the amount of climatic diversity within any of the regions. Figure 2 shows a map of North America with the eight geographical regions examined and the borehole sites. The numbers of temperature logs available for analysis in each region are enough to ensure robust trends, even when the data is sparse and unevenly distributed [*Beltrami et al.*, 1997; *Pollack and Smerdon*, 2004]. The quantity of boreholes in each region is given in Table 1. The majority of the Canadian boreholes were logged by GEOTOP at Université du Québec à Montréal (UQAM) in collaboration with the Institut de Physique du Globe (IPG, France) [*Beltrami and Mareschal*, 1991; *Mareschal et al.*, 2000, and references therein], and the Earth Physics Branch [*Jessop*, 1971] in holes of opportunity, thus the distribution is uneven. All data are available in the International Heat Flow Commission database.

2. Theory

[21] The temperature, $T(z)$, in a homogeneous, source-free, semi-infinite half-space, at a depth z is the superposition of the quasi-steady state temperature, T_0, the geothermal heat flow, q_0, and the temperature perturbation due to changes in the ground surface temperature (GST) T_t (z, t) [*Carslaw and Jaeger*, 1959] such that

$$T(z,t) = T_0 + q_0 R(z) + T_t(z,t), \tag{1}$$

where q_0 is the quasi-steady state surface heat flow density and $R(z)$ is the thermal depth. For a step change in temperature at the surface, the temperature perturbation, $T_t(z, t)$, is defined as

$$T_t = T_0 \mathrm{erfc}\left(\frac{z}{2\sqrt{\kappa t}}\right), \tag{2}$$

where erfc is the complementary error function, and κ is the thermal diffusivity of the subsurface medium. Evaluating the subsurface thermal profile with a known surface boundary condition is referred to as the forward problem. Conversely, the inverse problem determines the boundary condition, or ground surface temperature history (GSTH),

Table 1. Quantities of Boreholes and ECHO-g Grid Points Contained in Each Region[a]

Region	Number of Boreholes	Number of Grid Points
Pacific Canada	23	10
Western Canada	72	6
Central Canada	73	7
Atlantic Canada	14	2
California	5	2
Nevada	22	1
Intermountain West	43	9
Eastern United States	35	12

[a]In each of these regions, all boreholes and all ECHO-g grid points were averaged together to obtain the average subsurface temperature perturbation (TP) profile and the average ECHO-g simulated time series, respectively.

given the subsurface temperature perturbation profile [*Beltrami et al.*, 1997]. If the GST variations are approximated as a series of k step changes in temperature at the surface, the solution to the forward problem can be written as [*Mareschal and Beltrami*, 1992]

$$T_t(z) = \sum_{k=1}^{K} T_k \left[\mathrm{erfc}\left(\frac{z}{2\sqrt{\kappa t_k}}\right) - \mathrm{erfc}\left(\frac{z}{2\sqrt{\kappa t_{k-1}}}\right)\right], \qquad (3)$$

where T_k is the temperature of the kth step, and t_k is the time of the kth step. Equation (3) is used to generate forward modeled profiles using ECHO-g simulations as the driving upper boundary condition [*Beltrami et al.*, 2006b].

3. Analysis

[22] For all 287 boreholes used in this study, the subsurface temperature perturbation (TP) profile is obtained from each borehole temperature log by subtracting from it the quasi-steady state temperature. Because of geographical variations in microclimate and the diffusive nature of subsurface heat transport, boreholes record temperature anomalies pertinent to an area that is orders of magnitude smaller than the ECHO-g model spatial resolution. Individual boreholes, even those in close proximity, can show a high degree of variability in the thermal profiles recorded in the subsurface [*Beltrami et al.*, 2005]. Owing to differences in microclimate, elevation, groundwater flow, and precipitation regime, two boreholes separated by as little as 1 km can possess very different microclimates and microclimatic histories. This local variability is well known [*Beltrami and Mareschal*, 1992; *Clauser and Mareschal*, 1995; *Harris and Chapman*, 1995; *Pollack et al.*, 1996; *Beltrami et al.*, 1997; *Beltrami*, 2002b] and presents a problem when comparing sparsely populated borehole data with the regularly spaced output from a GCM.

[23] To overcome this obstacle and compare borehole data with model output in a meaningful way, eight regions of North America with relatively high borehole densities were outlined to attempt a regional comparison between the averages of the temperature profile for a region, and the nearby ECHO-g temperature-time series. In each geographical region, all borehole thermal profiles meeting predetermined depth range requirements of 200 to 700 m were averaged to obtain a representative temperature perturbation profile for the region [*Beltrami and Mareschal*, 1992; *Beltrami et al.*, 1992; *Clauser and Mareschal*, 1995; *Pollack et al.*, 1996; *Beltrami et al.*, 1997]. Figure 3 shows the ensemble of borehole temperature anomaly profiles and the average temperature perturbation profile for each region. With the exception of region e, all average temperature perturbation profiles are positive in the upper 200 m of the subsurface, and six out of eight show long-term warming trends indicating a sustained increase in underground heat content.

[24] The output from each integration of ECHO-g is a 1000-year annually resolved temperature-time series for every grid point on a 96 $\times$ 48 point lattice spanning the globe. All grid points within each region were averaged together to construct a representative model temperature-time series. The number of grid points averaged for each region are summarized in Table 1. The forward model is then applied to each of these regional temperature-time series to obtain the simulated subsurface temperature perturbation profile. In other words, we generate the expected anomalies in the thermal regime of the subsurface that result when the modeled paleoclimate temperatures are used as the driving upper boundary condition for each of these regions.

[25] Comparison of model simulations with subsurface temperature observations is not straight forward. To compare borehole temperature data and forward diffused paleoclimatic simulations using the forward model [*Beltrami et al.*, 2006b] a temporal reference period is needed to establish a context for changes in trend. This value is required for the simulated time series in order to calculate the model temperature anomalies which are subsequently forward diffused into the ground.

[26] This problem is similar to that of comparing instrumental time series with borehole TP profiles [*Harris and Gosnold*, 1999; *Harris and Chapman*, 2001, 2005]. In both cases the selection of a reference period is not evident because boreholes integrate a much longer climate history than the approximately two-century-long instrumental period or even the 1000-year GCM paleoclimatic simulations considered here. The contribution of this background or preobservational climate has been taken into account in exercises of comparisons between real borehole TP profiles and instrumental data making use of the preobservational mean (POM) concept [*Harris and Gosnold*, 1999; *Harris and Chapman*, 2001, 2005]. In the POM approach the selection of an elusive reference period with respect to which anomalies should be calculated is avoided and substituted by a search for an average temperature level (POM) which represents the contribution of the preobservational/instrumental local climate to the observed subsurface thermal regime. Therefore the uncertainty on the selection of a reference period can be overcome by scanning over a range of all possible mean temperature reference levels.

[27] The use of such an approach in the case of instrumental time series and borehole temperature profile comparisons is based in the assumption that GSTs and SATs track each other. Therefore the search for the appropriate POM level is performed by minimizing a measure of similarity between the diffused instrumental time series of temperature anomalies and the observed borehole temperature profiles. The selected POM value not only provides minimal error by definition, but this error is also expected to be very small in magnitude due to the assumed GST and SAT coupling. In the case of the comparison between actual and GCM forward diffused profiles this rationale cannot be sustained since millennial-long GCM simulations cannot be regarded as an exact representation of true past SAT. In fact, the figures described within the next section will show that different model simulations provide different climate realizations which ultimately translate into slightly different simulated borehole temperature profiles. Thus the strategy of searching for a minimal distance between real and simulated borehole temperature profiles cannot be designed under the rationale that the GCM-simulated thermal regimes will necessarily match the observed ones as in the comparisons between real boreholes and instrumental data. Yet, this approach is still useful as it allows scanning over a wide range of possible mean reference levels in the search for a

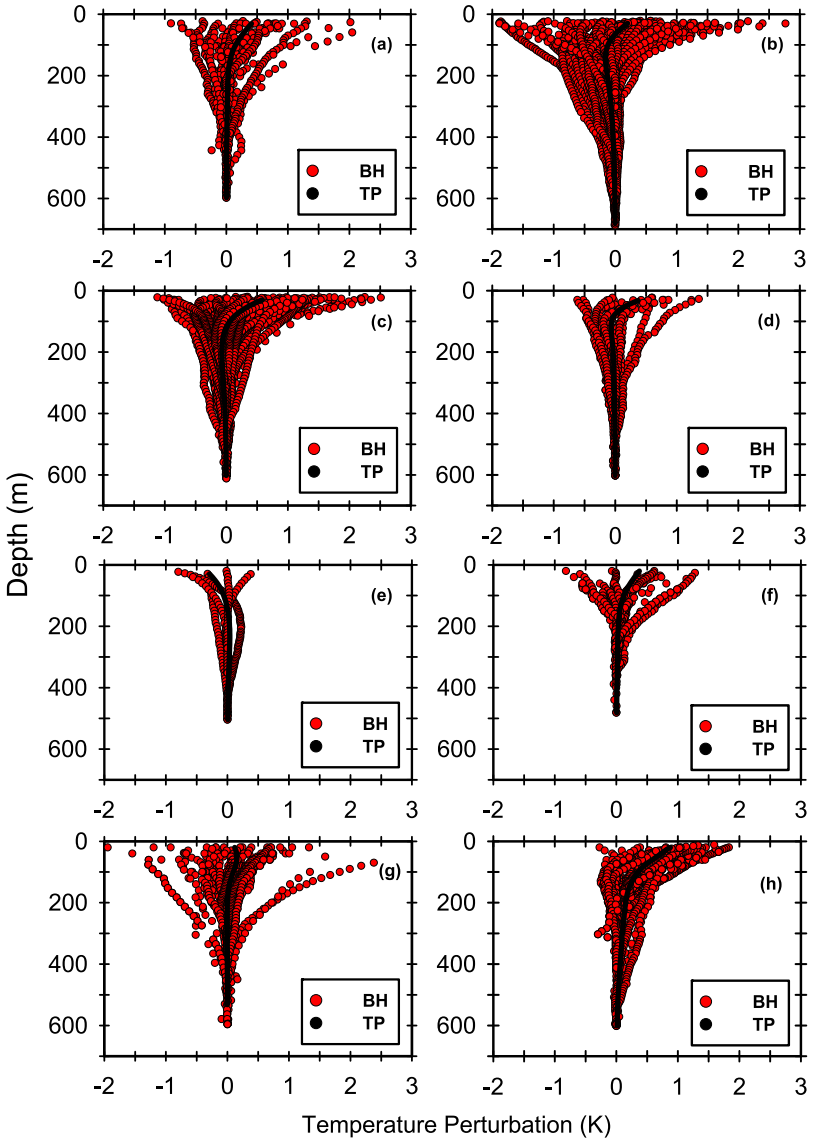

Figure 3. Illustrated is the spread of borehole data for each region (red) as well as the average temperature perturbation profile (black) of all borehole logs in each region. The average temperature perturbation profiles for each region show a dramatic increase in temperature recorded in the upper 150 m of the subsurface as well as varying degrees of cooling in the intermediate portions of the borehole depth. The plots are as follows: (a) Pacific Canada; (b) western Canada; (c) central Canada; (d) Atlantic Canada; (e) California; (f) Nevada; (g) intermountain West; and (h) eastern United States.

clear temporal reference period with respect to which simulated temperature anomalies can be calculated and forward diffused into the ground.

[28] In this fashion, a family of curves can be generated for each selected region by driving the forward model with a series of simulated SAT anomalies from a range of mean temperature reference levels. This family of curves illustrates the uncertainty in the selection of a temporal reference period in each model simulation and any measures of similarity (distance) between actual boreholes and the GCM-simulated TP profiles serve as a means of model-data comparison. This strategy has been used in this text as a first exercise to find an answer for a basic question, namely whether boreholes are more consistent with a control climate which considers only internal variability or whether the subsurface temperature anomalies are better explained by paleoclimatic simulations that include external (natural and anthropogenic) forcings. This is done by providing measures of similarity between observed and ECHO-g simulated (control and forced) borehole TP profiles. The proposed question is not futile in its simplicity since attempting an answer in this paper allows for designing a rationale of GCM-borehole comparison and further contributes to elucidate whether boreholes present a clear response to external forcing and thus meaningful information in the context of a climate change discussion. A more elaborate approach would incorporate the comparison of real borehole profiles with model simulations under the influence of

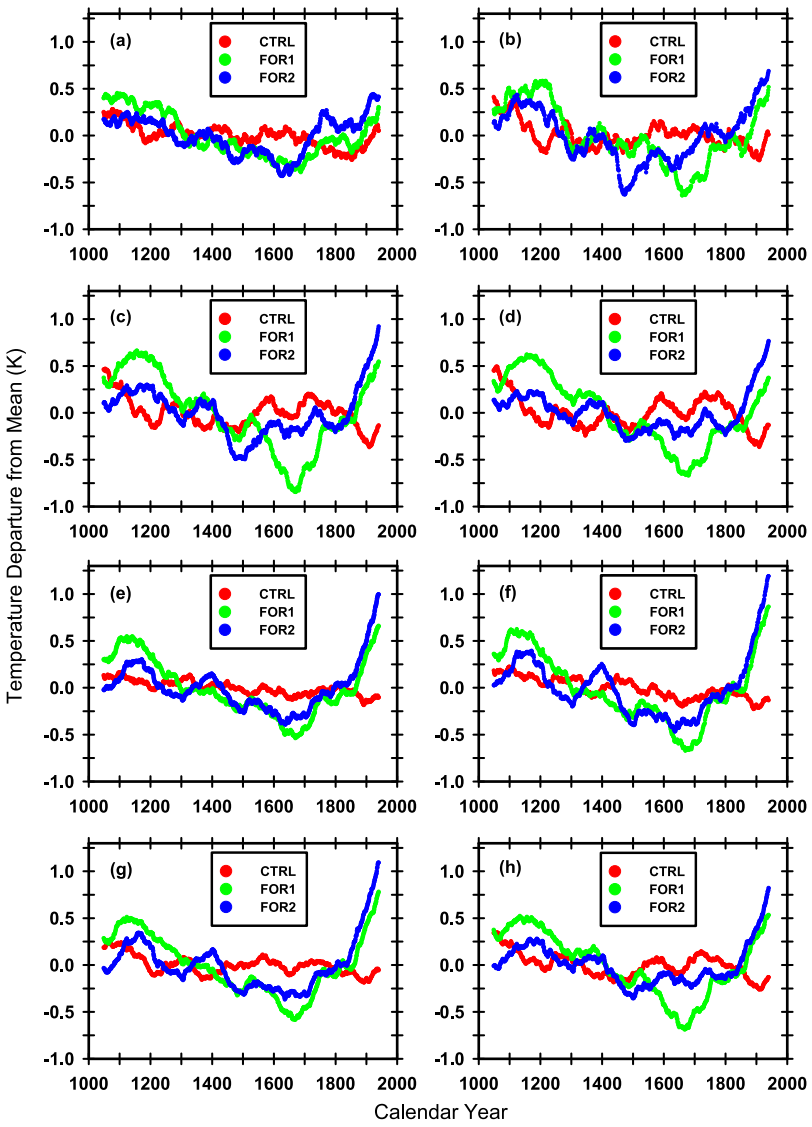

Figure 4. Shown are the ECHO-g simulated regional average temperatures expressed as departures from the mean of the entire simulation period. This plot has been smoothed for viewing clarity. The plots are as follows: (a) Pacific Canada, (b) western Canada, (c) central Canada, (d) Atlantic Canada, (e) California, (f) Nevada, (g) intermountain West, and (h) eastern United States.

forcings of different nature (anthropogenic versus natural) aiming at attributing causes for the observed trends. This orientation is beyond the scope of the present manuscript.

[29] The standard way to quantitatively explore how well two subsurface temperature anomaly profiles compare has been via their root mean square (RMS) difference. That is the absolute Euclidean distance in an *n*-dimensional space, where n is the number of data contained within each of the data sets being tested. This was the approach taken in *Beltrami et al.* [2006b] to facilitate an initial comparison of Canadian boreholes with ECHO-g simulations. However, RMS analysis on subsurface temperature profiles is difficult to interpret because of the nature of heat diffusion which attenuates signals nonlinearly as a function of depth, and also because, although the search targets the lowest RMS values in the comparison of real and simulated boreholes, these RMS values can still be relatively large in comparison with real data cases. Here we do not expect to perfectly reproduce reality at regional scales with small RMS values, but rather to use it as a relative distance measurement that will tell us what is closer to reality: the forward modeled subsurface anomalies from the control or forced simulations. Additionally, the goodness of fit is further assessed by using two additional criteria that complement the RMS analysis and strengthen our model and observation comparison: one is based on characterizing the depth at which the temperature gradient changes and the other establishes the magnitude of temperature change from this depth to the surface.

4. Results

[30] For a first-order comparison, the reference period for the ECHO-g model data was selected to be the entire data

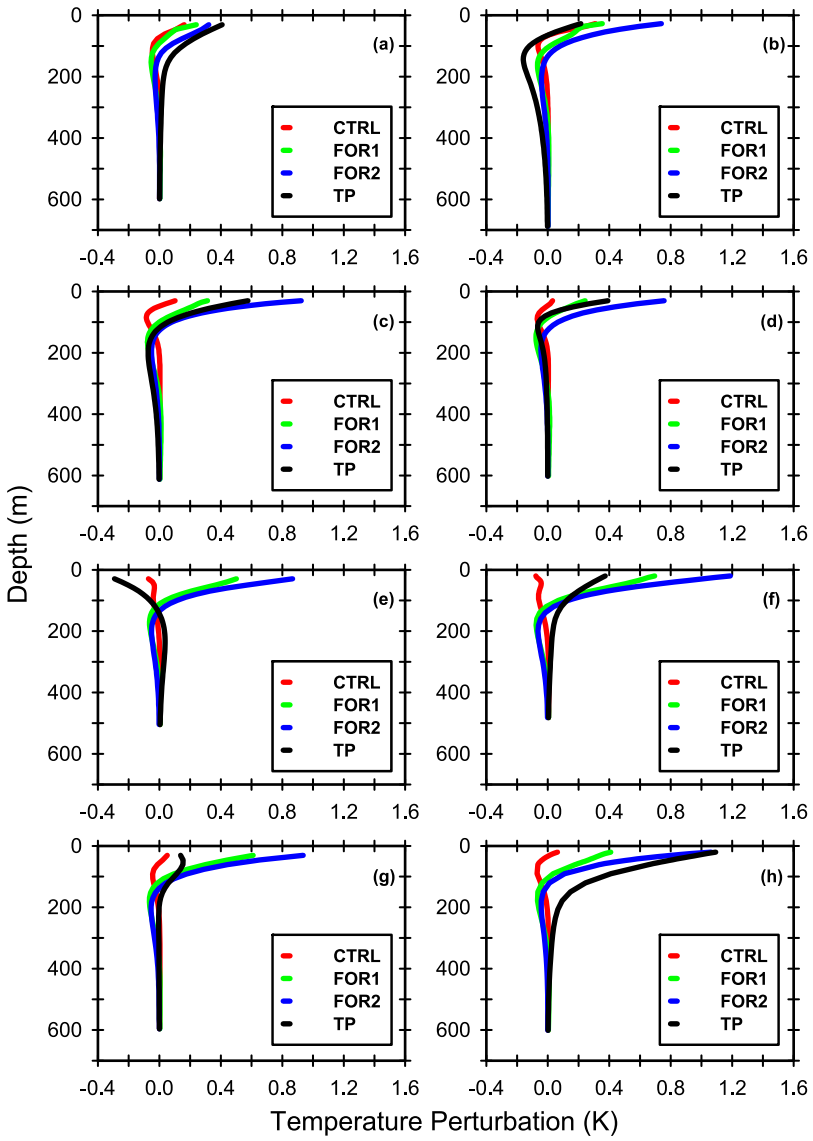

Figure 5. The forward modeled profiles from the three integrations of ECHO-g for (a) Pacific Canada, (b) western Canada, (c) central Canada, (d) Atlantic Canada, (e) California, (f) Nevada, (g) intermountain West, and (h) eastern United States. These forward modeled profiles are generated from ECHO-g 1000-year paleoclimatic simulations, with the entire period used as reference. Observed subsurface temperature anomalies are also shown.

series as in *Beltrami et al.* [2006b]. Figure 4 illustrates these model simulations referenced to this mean.

[31] The comparison results of the forward modeled ECHO-g regional means in Figure 4 and the mean regional subsurface TP profiles of Figure 3 are shown in Figure 5. Each panel shows the regional average TP profile in black, and the corresponding forward modeled profiles of the ECHO-g integrations CTRL, FOR1 and FOR2 in red, green and blue, respectively.

[32] Most of the forward modeled profiles show a pronounced reversal in long-term surface temperature trend between 100 m and 200 m in depth. Indeed, all average forward modeled profiles for the forced runs FOR1 and FOR2 show warming in the upper portions of the profile; profiles from CTRL either show a lesser degree of warming or none. To approximate this depth in a systematic way, a two-segment, piecewise regression (2R) was performed on each profile using RMS difference as the determinant of best fit [*Sollow*, 1987, 1995]. By truncating the profiles to 300 m prior to determining the 2*R* fit, only the shallower, less diffused portion of the profiles was used in fitting. Once the depth of trend reversal (δ) has been determined, the magnitude of temperature change since reversal (τ) can be determined by

$$\tau = T_z(z_i) - T_z(\delta), \tag{4}$$

where z_i is the shallowest depth in the profile log.

[33] Figure 6 illustrates the three criteria for assessing the degree of similarity between forward modeled temperatures and subsurface TP profiles shown in Figure 5. The RMS difference between the TP profile and each forward mod-

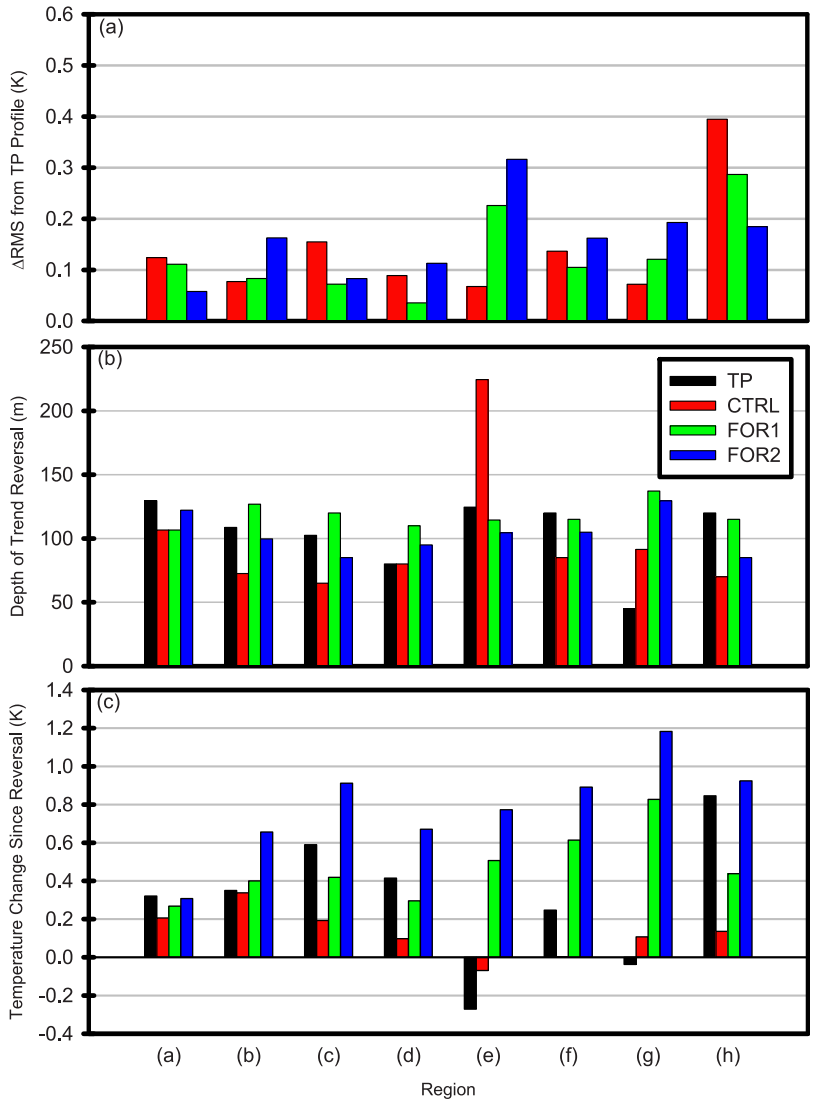

Figure 6. (a) RMS differences between forward modeled profiles and observations from the three integrations of ECHO-g when selecting the entire simulation as the reference period. Labels refer to the same regions as in Figure 2. (b) Depth at which the largest trend in the profiles reverses. (c) Magnitude of the temperature change after trend reversal. See text for explanation.

eled profile (Δ RMS) are shown for each region in Figure 6a. From this plot, it can be seen that in regions a, c, d, f, and h, the CTRL profile has the largest relative Δ RMS of the three ECHO-g integrations when compared to the TP profile. In regions b, e, and g, the opposite is true: the CTRL profile has the smallest relative Δ RMS of the three integrations compared to the TP profile. Figure 6b shows the subsurface depth at which the thermal gradient changes sign (δ), generally from a cooling to a warming trend. This is a common feature amongst most of the TP profiles and the forward modeled profiles. Generally, it can be seen that the δ values found in the TP profiles bear more resemblance to the δ values found in FOR1 and FOR2 than CTRL. Regions d and g show the only deviation from this generality. Finally, the magnitude of temperature change present in the subsurface profiles above the aforementioned depths (τ) is the subject of Figure 6c. Perhaps more difficult to interpret, the plot in Figure 6c clearly shows better agreement between TP and the forced simulations for the regions a, c, d, and h. The biggest discrepancies come from regions e and g, with both TP profiles showing cooling in the shallowest part of the profile. Regions b and f occupy a grey area that is somewhat open to interpretation, with τ values showing either good agreement with both CTRL and the forcing simulations, or splitting the difference between the two.

[34] For each of the three criteria considered above, there are more regions in which the average subsurface TP profile displays clear agreement with the ECHO-g forced runs than with the CTRL simulation. In the majority of cases, when the entire length of the ECHO-g paleoclimatic simulations is taken to be the reference period, the inclusion of realistic changes in forcing factors becomes necessary for an agreement to exist (see Figure 5).

[35] Since for the ECHO-g modeled temperatures, the proper reference period to calculate the temperature anoma-

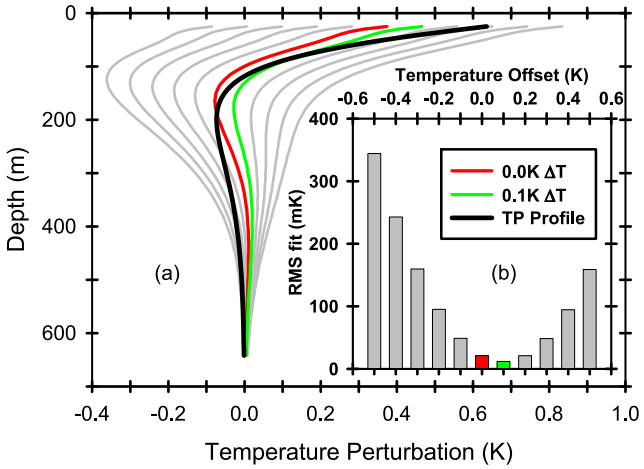

Figure 7. (a) Forward modeled profiles produced from simulation FOR1 for region c. The shaded curves show a set of forward modeled profiles generated from iterations through a range of reference temperatures. The observed temperature perturbation is shown in black. The forward modeled profile generated from the 1000-year mean as reference temperature is shown in red. The +0.1 K profile, which is the best comparison, is shown in green. (b) RMS values for all 11 forward modeled profiles in Figure 7a. The degree of agreement shows a quadratic relationship with initial temperature shift.

lies is unknown, the reference temperature itself was systematically altered from −0.5 K to +0.5 K in increments of 0.1 K. This was achieved by appending an initial temperature to the beginning of the model regional temperature simulation and iteratively reapplying the forward model. This method for comparing profiles is similar to the POM method used in detail in *Harris and Gosnold* [1999] and *Harris and Chapman* [2001, 2005]. Appending an initial temperature offset of +0.1 K is equivalent to changing the reference temperature of the time series by −0.1 K. Figure 7 shows how a forward modeled profile evolves as the initial temperature is systematically varied.

[36] By "mapping" the range of reference temperatures for a given region and model integration, a family of possible profiles emerges. To illustrate this, Figure 8 shows the family of profiles for region c (central Canada). As the reference temperature changes, so do the apparent depths of perturbations in the subsurface. Since this changes the magnitudes of trends in the time series relative to each other, the δ and τ values are altered accordingly.

[37] The same analysis is performed on the ranges of profiles as was conducted for the individual profiles generated using the entire length of simulated temperatures as the reference periods, and the results are displayed in Figure 9. Figure 9 shows Δ RMS values as in Figure 6a, but here the mean difference between the spread of profiles and the TP profile is plotted, with one standard deviation (σ). Differences between these means in each region are inconclusive within σ. It is for this reason that additional criteria for comparison are required. To aid in the comparison, the minimum Δ RMS values between the TP profile and one of the profiles from the spread are also plotted in Figure 9a. According to these values, the best-fitting forward modeled profile from each spread that best agrees with TP is one of the forcing runs for regions a, b, c, d, and h, and CTRL for regions e, f, and g.

[38] Figures 9b and 9c compare the respective mean δ and τ values for the three ECHO-g integrations with the average TP profile by region, also plotted with one standard deviation. Figure 9b shows that the δ values for TP show better agreement with either FOR1 or FOR2 than CTRL for regions a, b, c, e, f, and h. However, the perturbations in the TP profile of region e are opposite in sign to those of FOR1 and FOR2; inferring anything about their agreement is meaningless as the apparently good fit is coincidental. This emphasizes the need for multiple criteria when comparing average TP and forward modeled profiles. The noticeably larger error bars associated with the CTRL forward modeled profiles for regions e, f, and g illustrate the higher degree of variability between profiles with different reference periods in these regions. This instability is due to the fact that the CTRL simulation does not include variable external forcing factors, and is not subject to high-magnitude trends as in FOR1 and FOR2. Profiles with smaller trends have δ and τ values that are more sensitive to a change in reference period.

[39] The τ values in Figure 9c suggest a similar magnitude of warming to FOR1 or FOR2 for the regions a, c, d, and h. Regions e and g actually show trends of differing sign between TP and the forced runs, while region b shows good agreement between TP and both CTRL and FOR1. The TP profile from region f may be considered closer to FOR1 or FOR2 than CTRL due to the difference in the sign of subsurface anomalies between TP and CTRL.

[40] The results shown for the spread of profiles for each region are similar to those displayed for the case of the single profile derived from a 1000-year reference temperature. As before, for each of the three criteria discussed above, there are more regions displaying a clear agreement with the ECHO-g forced runs than with the CTRL simulation. Realistic changes in climatic forcing factors must be included in GCMs for there to be general agreement with subsurface thermal data obtained from boreholes (see Figure 9).

5. Discussion

[41] In general, the onset depth (δ) and postonset magnitude of temperature change since reversal (τ) preserved in the subsurface data is better reflected in the forcing profiles FOR1 and FOR2, and to a lesser extent or not at all in the CTRL profile. This means that the inclusion of variable forcing factors, such as greenhouse gas concentrations, is essential for plausibly simulating the climate of the last millennium. There are, however, a few deviations from this generality that complicate the interpretation of results.

[42] Figure 5e shows that California is the only region displaying a clear disagreement between the trends suggested by the ECHO-g simulations and those logged in boreholes. The source of this disagreement can be traced back to the dates of borehole logging. In the area of California the average year for borehole logging is 1966. Figure 10 shows the evolution of temperature anomalies throughout the 20th century in this region using data from two data sets, the CRU TS 2.1 [*Mitchell and Jones*, 2005]

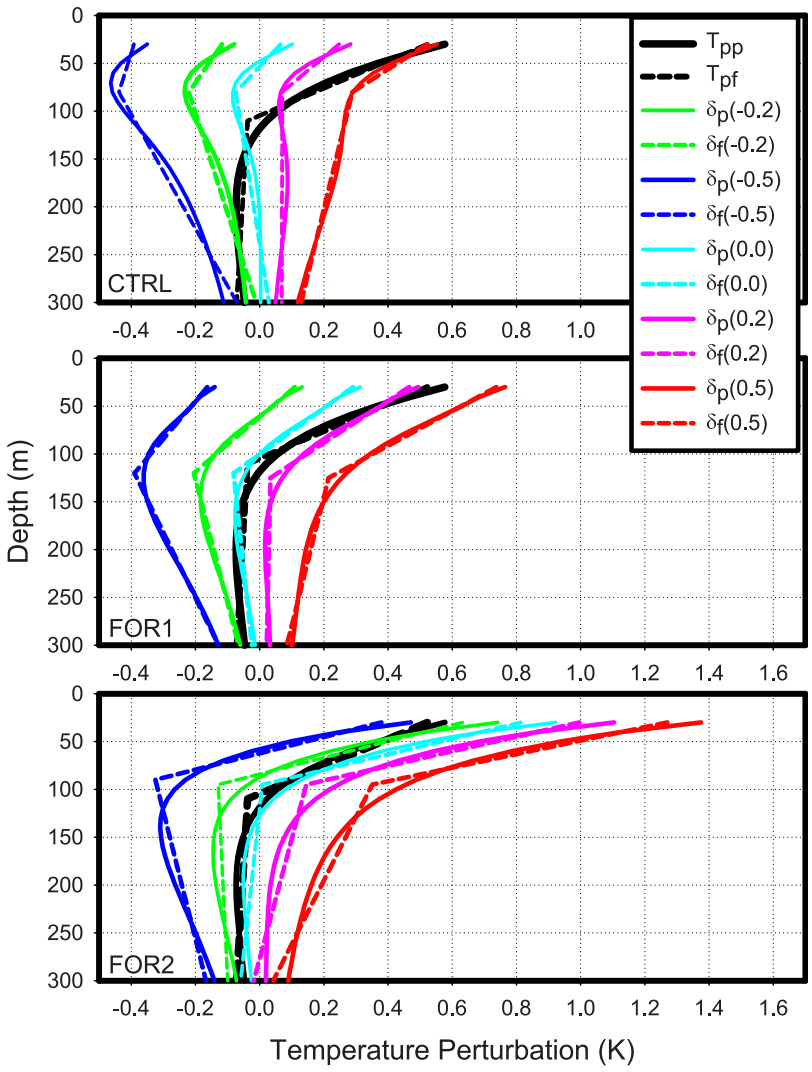

Figure 8. Illustration of the depth of trend reversal for selected forward modeled profiles for (a) CTRL, (b) FOR1, and (c) FOR2. The depth of trend reversal was found by computing the best fitting pair of regression lines to the profile. From this depth to the surface, the magnitude of temperature change since trend reversal can be established.

and the United States Historical Climatology Network (USHCN) [*Peterson et al.*, 1998; *Easterling et al.*, 1999]. The long-term trends over the 20th century in both climate histories are not identical. This can be related to different issues like calibration problems [*Hubbard and Lin*, 2006] or the questionable reliability of the very low frequency in the CRU TS 2.1 [*Mitchell and Jones*, 2005]. Both data sets, however, show good agreement in the representation of the decadal regional temperature changes. Before the average logging dates in the mid 1960s, the surface air temperature evolution indicates a clear cooling of approximately 0.4 K from 1926 to 1965, in agreement with the cooling (0.4 K) recorded in the subsurface TP in the area. After this period of cooling, temperature anomalies show a positive long-term increase to the present. If we consider the temperature evolution from the late 1970s to the present, the positive trends qualitatively support the ECHO-g behavior shown in Figure 5e. Quantitatively, the warming trend through the 20th century in the USHCN data (1.1 K) is consistent with those of the FOR1 (1.0 K) and FOR2 (1.3 K) simulations for California in Figure 10. It is also possible that the smaller borehole data set for California contributes to the lack of agreement with ECHO-g paleoclimate data.

[43] Another possible contributing factor to the discrepancy between the cooling shown in Californian boreholes and the nearby ECHO-g grids is the presence of high-density irrigation in California's Central Valley region. *Kueppers et al.* [2007] shows that irrigation at such an intense level appears to be driving the regional climatic signal into a sustained, multidecadal cooling trend, very similar to that shown in our borehole data set. There are no model parameters in ECHO-g to account for agricultural land use changes, including irrigation effects. This ICE would therefore not be observed in paleoclimate simulations using ECHO-g.

[44] The average TP profile of region g (intermountain West), illustrated in Figure 5g, shows a smaller RMS difference when compared to the CTRL profile than with

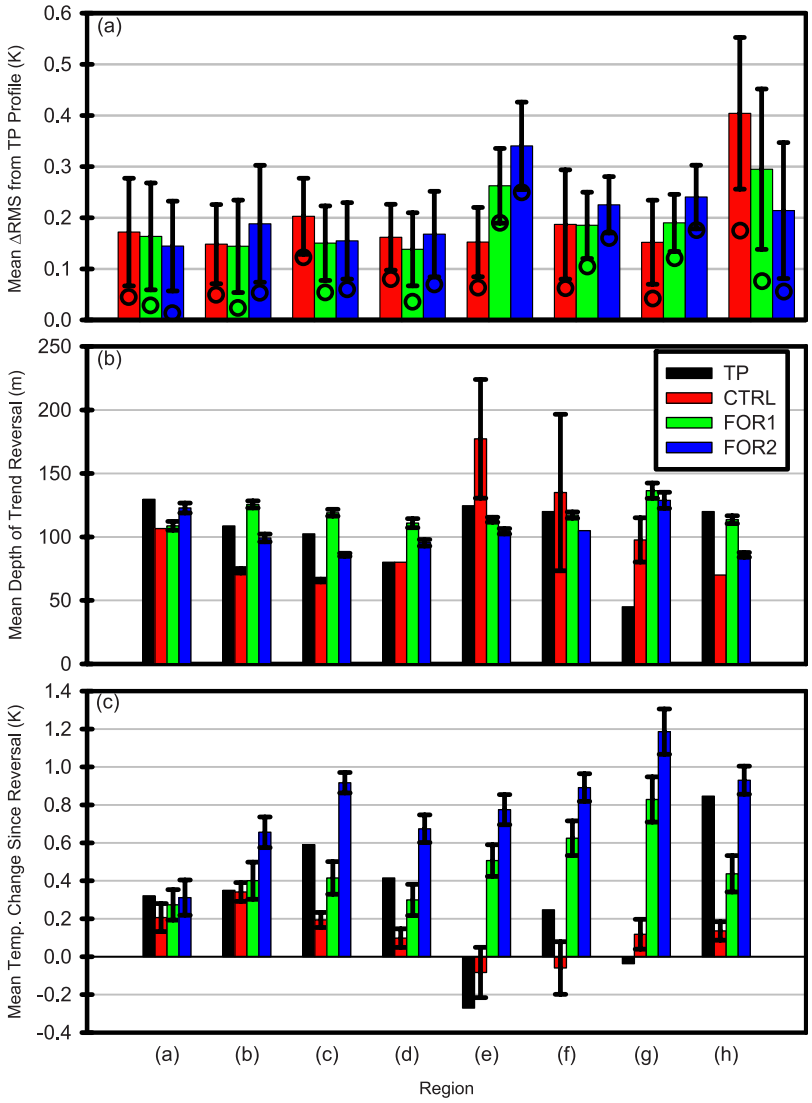

Figure 9. (a) Mean RMS differences between forward modeled profiles and observations from the three integrations of ECHO-g for a family of profiles generated using a range of reference periods. Also shown are the minimum RMS difference values from the spread of profiles (dots). Labels refer to the same regions as in Figure 2. (b) Depth at which the largest trend in the profiles reverses. (c) Magnitude of the temperature change after trend reversal. See text for explanation. Error bars show one standard deviation for all plots.

the profiles of either FOR1 or FOR2 (see Table 1). This might seem to suggest that there is agreement between TP and CTRL. This is in fact not the case. Although the magnitude and onset of perturbations in both profiles is similar, each pair of perturbations between the two profiles are opposite in sign. This implies that the two profiles are the result of opposite climate histories, which is unlikely. Even though the RMS difference between TP and CTRL is smaller than between TP and either FOR1 or FOR2, there is less structural similarity, ie., a gradual cooling from 600 m until 200 m followed by a rapid warming. In fact, the mean date of the logging of the boreholes in the intermountain West is 1967, and an examination of the meteorological records reveals the existence of a cooling period from the mid-1920s to 1970, so that the situation described for California also applies to this region. In general the distribution of the dates of borehole logging does not affect the ground surface temperature history reconstructed from subsurface temperatures [*González-Rouco et al.*, 2008].

[45] In the majority of cases, the closest forward profiles to the observations are those simulated subsurface anomalies obtained from the forced simulations rather than from the CTRL. This implies that the observed borehole subsurface temperature anomalies do not seem to arise only from internal variability of the climate system as modeled by the ECHO-g CTRL simulation. It appears that inclusion of realistic changes in forcings, as those included in simulations FOR1 and FOR2, are needed to explain the observed subsurface anomalies in most regions. For the implementation of the forward problem and the generation of subsurface anomalies from ECHO-g, we treated the output from the numerical simulations as if they were SAT from obser-

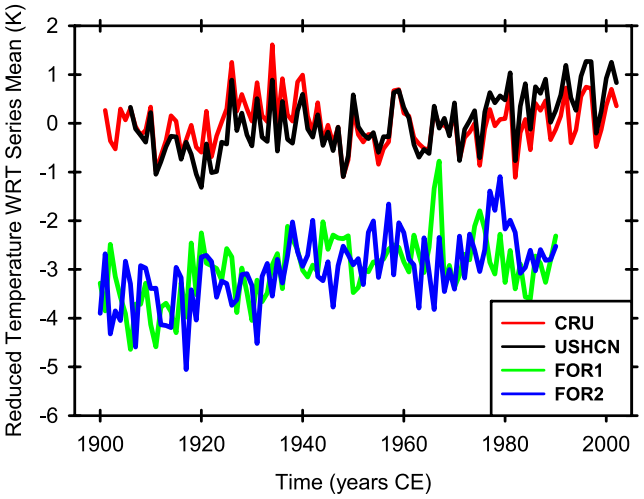

Figure 10. The 20th-century temperature anomaly histories for California from USHCN meteorological data (black), CRU interpolated data (red), and FOR1 and FOR2 from ECHO-g (green and blue, respectively, and both shifted down by 3 K for viewing clarity). The USHCN data have a clear warming over the 20th century, although the related CRU data do not. This suggests that the five borehole sites in California used in this study have very different climatic histories than the nearby meteorological

vations. Numerical simulations however, represent a possible climate scenario, internally consistent, and consistent with current climatology, but with an internal variability that could potentially be of the same order of magnitude as the initial temperature offset applied to each temperature-time series. Details of the agreement and disagreement between ECHO-g forward modeled temperatures, and observed underground anomalies may be able to help in understanding the internal dynamics of the model and the climate system. These sensitivities may allow for the improvement of the model's parameterizations to explain observations at regional resolution, as well as to improve model internal consistency in order to be able to use its output as a test base for proxy indicators of past climate reconstructions at regional levels [*von Storch et al.*, 2004].

[46] A better picture of past climate will probably be obtained from integrated analyses of paleoclimatic records and numerical models from which both disciplines will mutually benefit [*Trenberth and Otto-Bliesner*, 2003; *Beltrami et al.*, 2002, 2005; *González-Rouco et al.*, 2006; *Hansen et al.*, 2005; *von Storch et al.*, 2004, 2006].

6. Conclusion

[47] In each of eight North American geographical regions, all suitable boreholes were averaged together to create an average temperature perturbation profile. This profile was compared with three forward modeled temperature perturbation profiles: FOR1, FOR2 and CTRL.

[48] In most regions, the closest fitting profile to the TP profile is either FOR1, FOR2 or both. Since CTRL is a poorer fit in almost every case, it is clear that the inclusion of external forcing in a climate model is the difference between a model that describes the postindustrial long-term trends as recorded in the North American subsurface, and one that does not.

[49] Two of the regions, region e (California) and region g (the intermountain West), showed opposite behavior between the simulations and the borehole profiles. This disagreement is apparent and relates to the average date of logging in this area (mid 1960s). A closer inspection, taking into consideration the surface air temperature evolution in the area, supports the warming trends found in the simulations throughout the 20th century. In the remaining six regions, agreement between the average temperature perturbation profile obtained from subsurface temperature data and the externally forced runs FOR1 and FOR2 is significantly better than between subsurface data and the CTRL. All eight geographical regions clearly show that not only are boreholes sensitive to long-term climatic trends, but also external climatic forcing at the regional scale, such as variable greenhouse gas concentrations and solar flux. This realization further solidifies the role of subsurface temperature data as a robust record of paleoclimatic trends.

[50] Although ECHO-g was designed to simulate past climate on a global scale, the performance of runs FOR1 and FOR2 in this study strongly suggest that GCM simulations may be used to study long-term trends of past climate at the regional level. These simulations show potential for more thorough comparisons with observations when natural-only forced and anthropogenic-only forced simulations become available with ECHO-g or another model.

[51] **Acknowledgments.** This research was funded by the Natural Sciences and Engineering Research Council of Canada (NSERC), the Atlantic Innovation Fund (ACOA), and project CGL2005-06097 of the Spanish MEC. M.B.S. was partially funded by a graduate fellowship from the Atlantic Computing Excellence Network (ACEnet). Part of this work was carried out while J.F.G.R. was a James Chair Professor at STFX. J.F.G.R. was additionally funded by a Ramón y Cajal grant. Special thanks to Lisa Kellman, Asfaw Bekele, Dave Risk, and Nick Nickerson for insightful conversations and to Louise Bodri and Robert Harris for their thoughtful reviews of an earlier version of the manuscript.

References

Battle, M., et al. (1996), Atmospheric gas concentrations over the past century measured in air from firn at the South Pole, *Nature*, *383*, 231–235.

Bauer, E., and M. Claussen (2006), Analyzing seasonal temperature trends in forced climate simulations of the past millennium, *Geophys. Res. Lett.*, *33*, L02702, doi:10.1029/2005GL024593.

Bauer, E., M. Claussen, V. Brovkin, and A. Huenerbein (2003), Assessing climate forcings of the Earth system for the past millennium, *Geophys. Res. Lett.*, *30*(6), 1276, doi:10.1029/2002GL016639.

Beltrami, H. (2002a), Climate from borehole data: Energy fluxes and temperatures since 1500, *Geophys. Res. Lett.*, *29*(23), 2111, doi:10.1029/2002GL015702.

Beltrami, H. (2002b), Earth's long-term memory, *Science*, *297*, 206–207.

Beltrami, H., and E. Bourlon (2004), Ground warming patterns in the Northern Hemisphere during the last five centuries, *Earth Planet. Sci. Lett.*, *227*, 169–177.

Beltrami, H., and L. Kellman (2003), An examination of short- and long-term air-ground temperature coupling, *Global Planet. Change*, *38*, 291–303.

Beltrami, H., and J.-C. Mareschal (1991), Recent warming in eastern Canada inferred from geothermal measurements, *Geophys. Res. Lett.*, *18*, 605–608.

Beltrami, H., and J.-C. Mareschal (1992), Ground temperature histories for central and eastern Canada from geothermal measurements: Little Ice Age signature, *Geophys. Res. Lett.*, *19*, 689–692.

Beltrami, H., A. M. Jessop, and J.-C. Mareschal (1992), Ground temperature histories in eastern and central Canada from geothermal measurements: Evidence of climatic change, *Global Planet. Change*, *98*, 167–184.

Beltrami, H., L. Cheng, and J.-C. Mareschal (1997), Simultaneous inversion of borehole temperature data for past climate determination, *Geophys. J. Int.*, *129*, 311–318.

Beltrami, H., J. E. Smerdon, H. N. Pollack, and S. Huang (2002), Continental heat gain in the global climate system, *Geophys. Res. Lett.*, *29*(8), 1167, doi:10.1029/2001GL014310.

Beltrami, H., G. Ferguson, and R. N. Harris (2005), Long-term tracking of climate change by underground temperatures, *Geophys. Res. Lett.*, *32*, L19707, doi:10.1029/2005GL023714.

Beltrami, H., E. Bourlon, L. Kellman, and J. F. González-Rouco (2006a), Spatial patterns of ground heat gain in the Northern Hemisphere, *Geophys. Res. Lett.*, *33*, L06717, doi:10.1029/2006GL025676.

Beltrami, H., J. F. González-Rouco, and M. B. Stevens (2006b), Subsurface temperatures during the last millennium: Model and observation, *Geophys. Res. Lett.*, *33*, L09705, doi:10.1029/2006GL026050.

Bodri, L., and V. Cermak (2005), Borehole temperature, climate change and pre-observational surface air temperature mean: Allowance for hydraulic conditions, *Global Planet. Change*, *45*, 265–276.

Carslaw, H. S., and J. C. Jaeger (1959), *Conduction of Heat in Solids*, 2nd ed., 510 pp., Oxford Univ. Press, New York.

Clauser, C., and J.-C. Mareschal (1995), Ground temperature history in Central Europe from borehole temperature data, *Geophys. J. Int.*, *121*, 805–817.

Cook, E. R. (1995), Temperature histories from tree rings and corals, *Clim. Dyn.*, *11*, 211–222.

Crowley, T. (2000), Causes of climate change over the past 1000 years, *Science*, *289*, 270–277.

Cubasch, U., R. Voss, G. C. Hegerl, J. Waszkewitz, and T. J. Crowley (1997), Simulation of the influence of solar radiation variations on the global climate with an ocean-atmosphere general circulation model, *Clim. Dyn.*, *13*, 757–767.

Easterling, D. R., T. R. Karl, J. H. Lawrimore, and S. A. Del Greco (1999), United States Historical Climatology Network daily temperature, precipitation, and snow data for 1871–1997, *Rep. ORNL/CDIAC-118, NDP-070*, Carbon Dioxide Infor. Anal. Cent. Oak Ridge Natl. Lab., Oak Ridge, Tenn.

Esper, J., E. R. Cook, and F. H. Schweingruberg (2002), Low-frequency signals in long tree-ring chronologies for reconstructing past temperature variability, *Science*, *295*, 2250–2253.

Esper, J., D. C. Frank, and R. J. S. Wilson (2004), Climate reconstructions: Low-frequency ambition and high-frequency ratification, *Eos Trans. AGU*, *85*(12), 113–120.

Etheridge, D., L. P. Steele, R. L. Langenfelds, R. J. Francey, J.-M. Barnola, and V. I. Morgan (1996), Natural and anthropogenic changes in atmospheric CO_2 over the last 1000 years from air in Antarctic ice and firn, *J. Geophys. Res.*, *101*, 4115–4128.

Etheridge, D., L. P. Steele, R. J. Francey, and R. L. Langenfelds (1998), Atmospheric methane between 1000 A.D. and present: Evidence of anthropogenic emissions and climate variability, *J. Geophys. Res.*, *103*, 15,979–15,994.

Ferguson, G., and H. Beltrami (2006), Transient lateral heat flow due to land-use changes, *Earth Planet. Sci. Lett.*, *242*, 217–222.

Ferguson, G., H. Beltrami, and A. Woodbury (2006), Perturbation of ground surface temperature reconstructions by groundwater flow, *Geophys. Res. Lett.*, *33*, L13708, doi:10.1029/2006GL026634.

González-Rouco, J. F., H. von Storch, and E. Zorita (2003), Deep soil temperature as proxy for surface air-temperature in a coupled model simulation of the last thousand years, *Geophys. Res. Lett.*, *30*(21), 2116, doi:10.1029/2003GL018264.

González-Rouco, J. F., H. Beltrami, E. Zorita, and H. von Storch (2006), Simulation and inversion of borehole temperature profiles in simulated climates: Spatial distribution and surface coupling, *Geophys. Res. Lett.*, *33*, L01703, doi:10.1029/2005GL024693.

González-Rouco, J. F., H. Beltrami, E. Zorita, and M. B. Stevens (2008), Borehole climatology: A discussion based on contributions from climate modeling, *Clim. Past. Discuss.*, in press.

Goosse, H., T. J. Crowley, E. Zorita, C. M. Ammannm, H. Renssen, and E. Driesschaert (2005), Modelling the climate of the last millennium: What causes the differences between simulations?, *Geophys. Res. Lett.*, *32*, L06710, doi:10.1029/2005GL022368.

Hansen, J., et al. (2005), Earth's energy imbalance: Confirmation and implications, *Science*, *308*, 1431–1435.

Hansen, J., M. Sato, R. Ruedy, K. Lo, D. W. Lea, and M. Medina-Elizade (2006), Global temperature change, *Proc. Natl. Acad. Sci. U.S.A.*, *103*, 14,288–14,293, doi:10.1073/pnas.0606291103.

Harris, R. N., and D. S. Chapman (1995), Climate change on the Colorado Plateau of eastern Utah inferred from borehole temperatures, *J. Geophys. Res.*, *100*, 6367–6381.

Harris, R. N., and D. S. Chapman (2001), Mid latitude (30°–60°N) climatic warming inferred by combining borehole temperature with surface air temperature, *Geophys. Res. Lett.*, *28*, 747–750.

Harris, R. N., and D. S. Chapman (2005), Borehole temperatures and tree-rings: Seasonality and estimates of extratropical Northern Hemispheric warming, *J. Geophys. Res.*, *110*, F04003, doi:10.1029/2005JF000303.

Harris, R. N., and W. D. Gosnold (1999), Comparisons of borehole temperature-depth profiles and surface air temperatures in the northern plains of the U.S., *Geophys. J. Int.*, *138*, 541–548, doi:10.1046/j.1365-246X.1999.00884.x.

Hegerl, G. C., T. J. Crowley, W. T. Hyde, and D. J. Frame (2006), Climate sensitivity constrained by temperature reconstructions over the past seven centuries, *Nature*, *440*, 1029–1032.

Hegerl, G. C., T. J. Crowley, M. Allen, W. T. Hyde, H. N. Pollack, J. E. Smerdon, and E. Zorita (2007), Detection of human influence on a new, validated 1500 year temperature reconstruction, *J. Clim.*, *20*, 650–666.

Huang, S., H. N. Pollack, and P.-Y. Shen (2000), Temperature trends over the past five centuries reconstructed from borehole temperatures, *Nature*, *403*, 756–758.

Hubbard, K. G., and X. Lin (2006), Reexamination of instrument change effects in the U.S. Historical Climatology Network, *Geophys. Res. Lett.*, *33*, L15710, doi:10.1029/2006GL027069.

Intergovernmental Panel on Climate Change (2001), *Climate Change 2001: The Scientific Basis: Contribution of Working Group I to the Third Assessment Report of the Intergovernmental Panel on Climate Change*, edited by J. T. Houghton et al., 881 pp., Cambridge Univ. Press, New York.

Intergovernmental Panel on Climate Change (2007a), *Climate Change 2007: The Physical Science Basis: Contribution of Working Group I to the Fourth Assessment Report of the Intergovernmental Panel on Climate Change*, edited by S. Solomon et al., Cambridge Univ. Press, New York.

Intergovernmental Panel on Climate Change (2007b), *Climate Change 2007: Climate Change Impacts, Adaptation and Vulnerability: Working Group II Contribution to the Intergovernmental Panel on Climate Change Fourth Assessment Report*, edited by N. Adger et al., Cambridge Univ. Press, New York, in press.

Jessop, A. M. (1971), The distribution of glacial perurbation of heat flow in Canada, *Can. J. Earth Sci.*, *5*, 61–68.

Jones, P. D., and M. Mann (2004), Climate over past millennia, *Rev. Geophys.*, *42*, RG2002, doi:10.1029/2003RG000143.

Kohl, T. (1998), Palaeoclimatic temperature signals—Can they be washed out?, *Tectonophysics*, *291*, 225–234.

Kohl, T. (1999), Transient thermal effects below complex topographies, *Tectonophysics*, *306*, 311–324.

Kueppers, L. M., M. A. Snyder, and L. C. Sloan (2007), Irrigation cooling effect: Regional climate forcing by land-use change, *Geophys. Res. Lett.*, *34*, L03703, doi:10.1029/2006GL028679.

Lean, J., J. Beer, and R. Bradley (1995), Reconstruction of solar irradiance since 1610: Implications for climate change, *Geophys. Res. Lett.*, *22*, 3195–3198.

Legutke, S., and R. Voss (1999), The Hamburg atmosphere-ocean coupled circulation model ECHO-g, *Tech. Rep. 18*, Ger. Clim. Comput. Cent., Hamburg, Germany.

Levitus, S., J. Antonov, J. Wang, T. L. Delworth, K. Dixon, and A. Broccoli (2001), Anthropogenic warming of the Earth's climate system, *Science*, *292*, 267–270.

Levitus, S., J. Antonov, and T. Boyer (2005), Warming of the world ocean, 1955–2003, *Geophys. Res. Lett.*, *32*, L02604, doi:10.1029/2004GL021592.

Mann, M. E., R. S. Bradley, and M. K. Hughes (1999), Northern Hemisphere temperatures during the past millennium: Inferences, uncertainties, and limitations, *Geophys. Res. Lett.*, *26*, 759–762.

Mann, M. E., S. Rutherford, E. Wahl, and C. Ammann (2005), Testing the fidelity of methods used in proxy-based reconstructions of past climate, *J. Clim.*, *18*, 4097–4107.

Mareschal, J.-C., and H. Beltrami (1992), Evidence for recent warming from perturbed geothermal gradients: Examples from eastern Canada, *Clim. Dyn.*, *6*, 135–143.

Mareschal, J.-C., C. Jaupart, C. Gariépy, L. Z. Cheng, L. Guillou-Frottier, G. Bienfait, and R. Lapointe (2000), Heat flow and deep thermal structure near the edge of the Canadaian Shield, *Can. J. Earth Sci.*, *37*, 399–414.

Mitchell, T. D., and P. D. Jones (2005), An improved method of constructing a database of monthly climate observations and associated high-resolution grids, *Int. J. Clim.*, *25*, 693–712.

Moberg, A., D. M. Sonechkin, K. Holmgren, N. M. Datsenko, and W. Karlen (2005), Highly variable Northern Hemisphere temperatures reconstructed from low- and high-resolution proxy data, *Nature*, *433*, 613–617.

Montoya, M., A. Griesel, A. Levermann, J. Mignot, M. Hofmann, A. Ganopolski, and S. Rahmstorf (2005), The Earth system model of intermediate complexity CLIMBER-3α. part I: Description and performance for present-day conditions, *Clim. Dyn.*, *25*, 237–263, doi:10.1007/s00382-005-0044-1.

Mottaghy, D., and V. Rath (2006), Latent heat effects in subsurface heat transport modelling and their impact on palaeotemperature reconstruc-

tions, *Geophys. J. Int.*, *164*, 236–245, doi:10.1111/j.1365-246X.2005.02843.x.

Nitoiu, D., and H. Beltrami (2005), Subsurface thermal effects of land use changes, *J. Geophys. Res.*, *110*, F01005, doi:10.1029/2004JF000151.

North, G. R., et al. (2006), *Surface Temperature Reconstructions for the Last 2000 Years*, Natl. Acad., Washington, D. C.

Osborn, T., S. C. B. Raper, and K. R. Briffa (2006), Simulated climate change during the last 1000 years: Comparing the ECHO-g general circulation model with the MAGICC simple climate model, *Clim. Dyn.*, *27*, 185–197, doi:10.1007/s00382-006-0129-5.

Peterson, T. C., R. Vose, R. Schmoyer, and V. Razuvaev (1998), Global Historical Climatology Network (GHCN) quality control of monthly temperature data, *Int. J. Climatol.*, *18*, 1169–1179.

Pollack, H. N., and S. Huang (2000), Climate reconstructions from subsurface temperatures, *Ann. Rev. Earth Planet. Sci.*, *28*, 339–365.

Pollack, H. N., and J. E. Smerdon (2004), Borehole climate reconstructions: Spatial structure and hemispheric averages, *J. Geophys. Res.*, *109*, D11106, doi:10.1029/2003JD004163.

Pollack, H. N., P.-Y. Shen, and S. Huang (1996), Inference of ground surface temperature history from subusurface temperature data: Interpreting ensembles of borehole logs, *Pure Appl. Geophys.*, *147*, 537–550.

Pollack, H. N., J. E. Smerdon, and P. E. van Keken (2005), Variable seasonal coupling between air and ground temperatures: A simple representation in terms of subsurface thermal diffusivity, *Geophys. Res. Lett.*, *32*, L15405, doi:10.1029/2005GL023869.

Roeckner, E., K. Arpe, L. Bengtsson, M. Christoph, M. Claussen, L. Dumenil, M. Esch, M. Giorgetta, U. Schlese, and U. Schulzweida (1996), The atmospheric general circulation model ECHAM4: Model description and simulation of present-day climate, *Rep. 218*, 99 pp., Max-Planck-Inst. für Meterologie, Hamburg, Germany.

Roeckner, E., L. Bengtsson, J. Feichter, J. Lelieveld, and H. Rodhe (1999), Transient climate change simulations with a coupled atmosphere-ocean GCM including the tropospheric sulfur cycle, *J. Clim.*, *12*, 3004–3032.

Smerdon, J. E., and M. Stieglitz (2006), Simulating heat transport of harmonic temperature signals in the Earth's shallow subsurface: Lower-boundary sensitivities, *Geophys. Res. Lett.*, *33*, L14402, doi:10.1029/2006GL026816.

Smerdon, J. E., H. N. Pollack, V. Cermak, J. W. Enz, M. Kresl, J. Safanda, and J. F. Wehmiller (2006), Daily, seasonal and annual relationships between air and subsurface temperatures, *J. Geophys. Res.*, *111*, D07101, doi:10.1029/2004JD005578.

Sollow, A. R. (1987), Testing for climate change: An application of the two-phase regression model, *J. Clim. Appl. Meteorol.*, *26*, 1401–1405.

Sollow, A. R. (1995), Testing for change in the frequency of El Niño events, *J. Clim.*, *8*, 2563–2566.

Stevens, M. B., J. F. González-Rouco, J. E. Smerdon, M. Stieglitz, and H. Beltrami (2007), Effects of bottom boundary placement on subsurface heat storage: Implications for climate model simulations, *Geophys. Res. Lett.*, *34*, L02702, doi:10.1029/2006GL028546.

Trenberth, K. E., and B. L. Otto-Bliesner (2003), Toward integrated reconstructions of past climates, *Science*, *300*, 589–591.

von Storch, H., E. Zorita, J. Jones, Y. Dimitriev, F. González-Rouco, and S. Tett (2004), Reconstructing past climate from noisy data, *Science*, *306*, 679–682.

von Storch, H., E. Zorita, J. Jones, F. González-Rouco, and S. F. B. Tett (2006), Response to the comment by Wahl, Ritson and Amman "Reconstruction of century scale temperature variations," *Science*, *312*, 529.

Warrilow, D. A., A. B. Sangster, and A. Slingo (1986), Modelling of land surface processes and their influence on European climate, *Tech. Note 20 DCTN 38*, Meteorol. Off., Bracknell, U.K.

Wolff, J. O., E. Meier-Reimer, and S. Legutke (1997), The Hamburg ocean primitive equation model, *Rep. 13*, 98 pp., German Clim. Comput. Cent., Hamburg, Germany.

Zhang, T. (2005), Influence of the seasonal snow cover on the ground thermal regime: An overview, *Rev. Geophys.*, *43*, RG4002, doi:10.1029/2004RG000157.

Zorita, E., J. F. González-Rouco, and S. Legutke (2003), Testing the Mann et al. (1999) approach to paleoclimate reconstructions in the context of a 1000Yr control simulation with the ECHO-g coupled climate model, *J. Clim.*, *16*, 1378–1390.

Zorita, E., H. von Storch, J. F. González-Rouco, J. Lutherbacher, U. Cubasch, S. Legutke, and U. Schlese (2004), Climate evolution in the last five centuries simulated by an atmosphere-ocean model: Global temperatures, the North Atlantic Oscillation and the Late Maunder Minimum, *Meteorol. Z.*, *13*, 271–289.

Zorita, E., J. F. González-Rouco, H. von Storch, J. P. Montávez, and F. Valero (2005), Natural and anthropogenic modes of surface temperature variations in the last thousand years, *Geophys. Res. Lett.*, *32*, L08707, doi:10.1029/2004GL021563.

H. Beltrami and M. B. Stevens, Environmental Sciences Research Centre, Department of Earth Sciences, St. Francis Xavier University, 1 West Street, Antigonish, Nova Scotia, Canada B2G 2W5. (hugo@esrc.stfx.ca)

J. F. González-Rouco, Departamento de Astrofísica y CC. de la Atmósfera, Universidad Complutense de Madrid, Madrid E-28040, Spain.